Pironetin binds covalently to αCys316 and perturbs a major loop and helix of α-tubulin to inhibit microtubule formation

Andrea E. Prota[1*], Jocelyn Setter[2], Andrew B. Waight[2], Katja Bargsten[1], Juan Murga[3], José Fernando Diaz[4] and Michel O. Steinmetz[1*]

[1]Laboratory of Biomolecular Research, Department of Biology and Chemistry, Paul Scherrer Institut, Villigen, Switzerland

[2]Department of Protein Sciences, Seattle Genetics, Inc., Bothell, WA, USA

[3]Depart. de Q. Inorgánica y Orgánica, Univ. Jaume I, E-12071 Castellón, Spain

[4]Chemical and Physical Biology, Centro de Investigaciones Biológicas, Consejo Superior de Investigaciones Científicas CIB-CSIC, Madrid, Spain.

[*]Corresponding authors: andrea.prota@psi.ch and michel.steinmetz@psi.ch

ABSTRACT

Microtubule-targeting agents are among the most powerful drugs used in chemotherapy to treat cancer patients. Pironetin is a natural product that displays promising anticancer properties by binding to and potently inhibiting tubulin assembly into microtubules; however, its molecular mechanism of action remained obscure. Here, we solved the crystal structure of the tubulin-pironetin complex and found that the compound covalently binds to Cys316 of α-tubulin. The structure further revealed that pironetin perturbs the T7 loop and helix H8 of α-tubulin. Since both these elements are essential for establishing longitudinal tubulin contacts in microtubules, this result explains how pironetin inhibits the formation of microtubules. Together, our data define the molecular details of the pironetin binding site, and thus offer a promising basis for the rational design of pironetin variants with improved activity profiles. They further extend our knowledge on strategies evolved by natural products to target and perturb the microtubule cytoskeleton.

Pironetin (Figure 1A) was originally isolated from fermentation broths of *Streptomyces* strains as a plant growth regulator[1; 2]. Subsequently, it was found that pironetin and its derivatives are potent inhibitors of microtubule formation, arrest cell cycle progression in mitosis and exhibit antitumor activity by inducing apoptosis[3; 4] Based on alanine scanning mutagenesis and a biotinylated derivative, it has been proposed that pironetin covalently binds to Lys352 of α-tubulin[5]. Using this information and in combination with molecular dynamics simulations, it has been further speculated that pironetin destabilizes microtubules by perturbing the formation of lateral tubulin contacts in microtubules[6]. We reasoned that a high-resolution structure of the tubulin-pironetin complex would provide a detailed description of how pironetin interacts with tubulin at the atomic level and establish a firm basis for the mechanism of action of the compound on tubulin and microtubules. In order to obtain this information, we soaked crystals of a protein complex composed of two αβ-tubulin heterodimers, the stathmin-like protein RB3 and tubulin tyrosine ligase[7; 8] (T_2R-TTL) with pironetin, and determined the structure of this quaternary complex by X-ray crystallography at 2.1 Å resolution (Table 1).

Pironetin binds to an extended hydrophobic cavity on α2-tubulin at the inter-dimer interface of the T_2R-TTL complex; the equivalent site on α1-tubulin is protected by the N-terminal β-hairpin of RB3 and did not react with pironetin in our crystal system (Figure 1BC). The overall structure of tubulin in the tubulin–pironetin complex superimposed well with the one obtained in the absence of the ligand[7] (PDB ID 4I55, $rmsd_{overall}$ of 0.3 Å over 1966 Cα atoms; $rmsd_{α2\text{-}Tub}$ of 0.1 Å over 317 Cα atoms). This result suggests that binding of the compound does not affect the global structure of the tubulin dimer, although we cannot exclude that the ligand may affect the conformation of the protein in its free state. In the tubulin-pironetin complex structure, the pyrone ring of the compound is perfectly oriented to allow for the formation of a covalent bond by Michael addition[9] between the C3 atom of pironetin and Cys316 of α-tubulin (Figure 1A). In addition, the carbonyl group of the pyrone ring forms the sole polar interaction through a water-mediated hydrogen bond to the backbone carbonyls of Ser237 and Ile238, and to the side chain OH group and backbone amide of Ser241 of α-tubulin. The ethyl group C15-C16 attached at position C4 of pironetin is deeply inserted into a pocket formed by residues Leu318, Ile238, Cys376 and Leu378 of α-tubulin. Consistent with its prominent role for binding, pironetin variants lacking this ethyl side chain, or where this moiety has been replaced by a methyl group, decreased the biological activities of the resulting compounds[10; 11]. The C6-C14 alkyl chain of pironetin is positioned such that both the C8 and C10 methyl groups are oriented towards two pockets formed by the side chains of Leu167, Cys200, Phe202, Ile238, Leu259, and Leu378, and Cys4, Phe52, Leu136, Phe169, Thr239 and Leu242 of α-tubulin, respectively (Figure 1CD). Furthermore, the terminal alkenyl moiety of pironetin is perfectly oriented to fit into a cavity

formed by residues Cys4, Gln133, Leu136, Ser165, Leu167, Leu242 and Gln256, thereby forming two weak hydrogen bonds to Cys4 and Gln256 of α-tubulin[12]. This observation underpins the critical role of the C12-C13 double bond in maintaining the precise conformation of pironetin for achieving its full biological activity[3; 4].

A key feature of the tubulin-pironetin interaction is the covalent binding of the compound to Cys316 of α-tubulin (Figure 1C). This result is in contrast to previous work that proposed Lys352 of α-tubulin as the target residue of a pironetin derivative in which a biotin moiety was attached to the O7 group of the compound[5]. Notably, we observed continuous density between the C3 atom of pironetin and Cys316 of α-tubulin in our crystal, which allows to unambiguously defining the covalent bond at this position (Figure 2A). In contrast, the Lys352 side chain displays poor electron density and is thus only partially ordered (Figure 2B). The tubulin-pironetin complex structure provides a possible explanation why covalent binding to Cys316 was not detected in the previously published experiments with the biotinylated pironetin derivative [5]: the biotin-moiety is expected to clash into the T7 loop and helix H8 of α-tubulin (Figure 1D). We noted that the activity of the biotinylated pironetin derivative is 50-fold less potent compared to the parent compound[5], suggesting that the biotin moiety indeed strongly affects binding of the pironetin derivative to tubulin and microtubules.

To verify that pironetin also binds covalently to Cys316 of α-tubulin in solution, we performed high-performance liquid chromatography (HPLC) experiments in combination with mass spectrometry (MS) analyses. When intact αβ-tubulin heterodimers were analyzed by HPLC in denaturing conditions, the α- and β-tubulin subunits resolved from each other, with β-tubulin eluting first (Figure 2C). When this chromatographic separation is coupled to high-resolution MS, the heterogeneous nature of post-translational modifications known to exist on tubulin is revealed[13]. Following incubation with pironetin, a clear chromatographic shift of the α-tubulin peak is observed (Figure 2C). This result suggests that pironetin is irreversibly bound to α-tubulin, and deconvolution of the mass spectra demonstrates a mass shift consistent with one pironetin molecule covalently attached to α-tubulin. In contrast, there was no observed mass or retention time shift for β-tubulin in the untreated control.

In order to determine the specific amino acid that is being covalently modified by pironetin, a tubulin-pironetin mixture was subjected to enzymatic digestion and peptide mapping utilizing ultra-performance liquid chromatography (UPLC) coupled to high-resolution MS. *In silico* digestion of αβ-tubulin was used to predict the peptide that contains Cys316 of α-tubulin (residues 306-321) and has an expected monoisotopic mass of 2263.132 Da when covalently modified by pironetin. Using this mass to generate an extracted ion chromatogram from the total ion chromatogram of the peptide map, a single peak with a measured mass of 2263.155 Da (10 ppm mass accuracy, calculated from 2^+ and 3^+ charge states) is observed at a retention time of 7.08 min (Figure 2D). This peak was not

observed in the tubulin control (not shown). When the mass of the peptide containing pironetin addition at Lys352 of α-tubulin was queried (residues 345-366, 2712.387 Da), there were no observed peaks above background (Supplemental Figure 1). To verify that this result is not a false negative and that the peptide could successfully be analyzed by this technique, the mass of the unmodified peptide was queried and found to be present with a high degree of mass accuracy in both the treated and untreated tubulin samples (Supplemental Figure 1). The results from the peptide map analysis confirms that pironetin indeed covalently reacts with the α-tubulin peptide containing Cys316 and shows no evidence of modification at Lys352; although this analysis does not elucidate the specific amino acid residue on which pironetin is attached. To define the exact residue, LC-MS/MS analysis was performed using the same peptide mixture described above. The peptides were once again resolved by UPLC coupled to MS and the mass of the peptide containing Cys316 and the pironetin modification was selected for isolation and fragmentation in the collision cell. The subsequent MS/MS spectra generated was deconvoluted and manually interpreted. A complete y-ion series ranging from y2-y10 was observed (with an average 6 ppm mass accuracy across the series) and demonstrated that pironetin is indeed covalently bound to Cys316 of α-tubulin, as observed in the crystal structure of the tubulin-pironetin complex (Figure 2AE).

Next, we sought to investigate how exactly pironetin inhibits tubulin assembly into microtubules. In the non-liganded state, the T7 loop and helix H8 of α-tubulin are well defined and pack against the central beta-sheet of the protein, whereby the side chains of Leu252 and Phe255 of helix H8 pack into a hydrophobic cavity formed by residues Leu167, Phe202, Ile238, Leu242 and Val250, Lys352, Cys316 and Leu318, respectively (Figure 3AC). In the tubulin-pironetin complex, both the C8 and C10 methyl and the C9 methoxy groups of pironetin cover a space at the entrance of two pockets that is otherwise occupied by the side chain of Leu252 in the unliganded α-tubulin structure. As a consequence, both Leu252 and Phe255 residues are displaced upon pironetin binding, which causes a disordering of the T7 loop and a conformational perturbation in the N-terminal part of helix H8 (Figure 3BC) - we cannot exclude that the ligand induces greater conformational changes when bound to free tubulin. However, the finding that pironetin binds to a site that is normally not accessible from the solvent indicates that both the T7 loop and helix H8 of α-tubulin must have some degrees of dynamicity for the compound to access its binding site. Importantly, both these secondary structure elements contain five key residues, Ala247, Leu248, Asn249, Glu254 and Thr257, which establish longitudinal tubulin contacts in microtubules[14] (Figure 4A). We thus expect that pironetin destabilizes microtubules either by forming assembly incompetent tubulin–compound complexes with unassembled tubulin dimers at high ligand concentrations, or by directly binding to the minus ends of microtubules that expose α-tubulin subunits at substoichiometric, therapeutically relevant compound concentrations, thus inhibiting the addition of further tubulin dimers (Figure 4B).

In conclusion, our results establish that pironetin binds covalently to Cys316 of α-tubulin. The data further suggest that the compound prevents tubulin assembly by inhibiting longitudinal tubulin contacts in microtubules. Notably, the molecular mechanism of action of pironetin on tubulin and microtubules (Figure 4B) is different from the ones described for the other three known classes of microtubule-destabilizing agents: (i) Colchicine-site ligands prevent the intra-dimer 'curved-to-straight' conformational change that must occur upon tubulin incorporation into microtubules[15]; (ii) Vinca-site compounds destabilize microtubules by introducing a wedge at the inter-dimer interface between two tubulin molecules at the tips of microtubules, thereby inhibiting the curved-to-straight conformational transition, or by stabilizing curved, ring-like oligomers that are not compatible with the straight tubulin structure found in microtubules[16]; (iii) Maytansine-site ligands bind to β-tubulin and directly block the formation of longitudinal tubulin contacts in microtubules[17]; at substoichiometric compound concentrations, and in contrast to pironetin, they may thus poison the plus ends of microtubules. Taken together, our study extends our knowledge on the portfolio of mechanisms evolved by natural products that perturb the microtubule cytoskeleton. They further offer a rational basis for the development of new pironetin variants with improved activity profiles.

MATERIALS AND METHODS

Proteins and compounds

Bovine brain tubulin was prepared according to ref. [18]. Methods for the production of the T_2R-TTL complex using the stathmin-like domain of RB3 and chicken TTL expressed in *E. coli*, have been described previously[7; 8; 19].

Crystallization, data collection and structure solution

Crystals of T_2R-TTL were generated as described previously[7; 8]. Suitable T_2R-TTL crystals were soaked overnight in reservoir solutions containing 10% PEG 4K, 12% glycerol and 0.5 mM pironetin, and were flash cooled in liquid nitrogen following a brief stepwise transfer into cryo solutions containing 15% and 20% glycerol, respectively. T_2R-TTL-pironetin data were collected at beamline X06DA at the Swiss Light Source (Paul Scherrer Institut, Villigen, Switzerland). Images were indexed and processed using XDS[20], and structure solution by the difference Fourier method and refinement were performed using the PHENIX package[21]. Model building was carried out iteratively using the Coot software[22]. Data collection and refinement statistics are given in Table 1.

Intact, denaturing mass spectrometry (MS)

Sheep brain tubulin was diluted to 600 nM in a buffer consisting of 25 mM PIPES, pH 6.9, 1 mM $MgCl_2$ and 0.25 mM EGTA (General Tubulin Buffer (GTB)). Pironetin (1 mM DMSO stock) was allowed to react with tubulin in situ at a ten-fold excess concentration (6 µM) in the dark. Aliquots for each time point queried were analyzed on a Waters UPLC (H-class Acquity) coupled to a Waters G2-S QTof mass spectrometer and separated by an Agilent PLRP-S column (1000 Å; 8 µm; 4.6 x 50 mm) and the solvent system consisted of buffer A (0.05% TFA in water) and buffer B (0.01% TFA in acetonitrile). The loaded material was eluted from the column (heated at 80 °C) at a flow rate of 1.0 mL/min with the following gradient: linear 27–44% of B over 13.5 min and linear 44–27% of B for 2.5 min. The mass spectrometer was operated in resolution mode with a 500-4000 m/z mass range, 1 second scan time and a collision energy equaling 10 V.

Peptide map MS and analysis

Following overnight reaction of tubulin with pironetin as described above, the modified tubulin was stored at -80 °C prior to enzymatic digestion with Asp-N. The tubulin-pironetin mixture was thawed, and naïve tubulin was carried through the remaining steps as a control. Guanidine was added to each sample to a final concentration of 6 M in order to denature the protein. The samples were then reduced with 5 mM DTT and alkylated via subsequent addition IAA at a final concentration of 15 mM. The reaction was quenched by incubation at 20 mM DTT. The excess reagents were removed by performing 5 rounds of concentration in 10 kDa spin filters and dilution with 100 mM Tris-HCl, pH 7.4. AspN (Promega Sequencing Grade) was added to each sample at 1:100 w/w and incubated for 4 hours at 37 °C. The digestion was stopped by freezing at -80 °C. An aliquot of 10 µg for each sample was injected utilizing the same generic UPLC-MS setup described above. The peptides were resolved on to a Zorbax StableBond C8 UPLC column (300 Å; 1.8 µm; 2.1 x 50 mm) and the solvent system consisted of buffer A (0.1% TFA in water) and buffer B (0.08% TFA in acetonitrile). The loaded material was eluted from the column (heated at 60 °C) at a flow rate of 0.624 mL/min with the following gradient: linear 0–39% of B over 7.81 min, linear 39-95% of B for 0.58 min, isocratic 95% of B for 0.42 min, linear 95–0% of B for 0.1 min and isocratic 0% of B for 0.76 min. To analyze intact peptides, the mass spectrometer was operated in sensitivity mode with a 200-2000 m/z mass range, 1 second scan time and a collision energy equaling 10 V. To perform LC-MS/MS on the peptides, the mass spectrometer was operated in resolution mode and a collision energy equaling 30 V. The MS scanning range was 50-2000 m/z with a 1 second scan time and the MS/MS scan settings were adjusted for each injection such that the set mass equaled the 3+ charge state of the peptide investigated.

Structural analysis and figure preparation

Molecular graphics and analyses were performed with PyMol (The PyMOL Molecular Graphics System, Version 1.5.0.5. Schrödinger, LLC). Chains in the T_2R-TTL complex were defined as follows: chain A, α1-tubulin (α1Tub); chain B, β1-tubulin (β1Tub); chain C, α2-tubulin (α2Tub); chain D, β2-tubulin (β2Tub); chain E, RB3; and chain F, TTL (Figure 1B).

Accession numbers

Coordinates and structure factors of the T_2R-TTL-pironetin complex structure have been deposited in the Protein Data Bank with accession number 5LA6.

ACKNOWLEDGMENTS

X-ray data were collected at beamline X06DA of the Swiss Light Source (Paul Scherrer Institut, Villigen, Switzerland). This work was supported by grants from the Ministerio de Economía y Competitividad and Conselleria d'Educaciò and Investigaciò, Cultura i Sport de la Generalitat Valenciana (CTQ2014-52949-P and PROMETEO 2013/027, respectively; to J.M.), from the Ministerio de Economia y Competitividad and Comunidad Autónoma de Madrid (BIO2013-42984-R and S2010/BMD-2457 BIPEDD2, respectively; to J.F.D), and from the Swiss National Science Foundation (310030B_138659 and 31003A_166608; to M.O.S.). The authors acknowledge networking contribution by the COST Action CM1407 "Challenging organic syntheses inspired by nature - from natural products chemistry to drug discovery" and the COST action CM1470.

REFERENCES

1. Kobayashi, S., Tsuchiya, K., Harada, T., Nishide, M., Kurokawa, T., Nakagawa, T., Shimada, N. & Kobayashi, K. (1994). Pironetin, a novel plant growth regulator produced by Streptomyces sp. NK10958. I. Taxonomy, production, isolation and preliminary characterization. *J Antibiot (Tokyo)* **47**, 697-702.
2. Kobayashi, S., Tsuchiya, K., Kurokawa, T., Nakagawa, T., Shimada, N. & Iitaka, Y. (1994). Pironetin, a novel plant growth regulator produced by Streptomyces sp. NK10958. II. Structural elucidation. *J Antibiot (Tokyo)* **47**, 703-7.
3. Kondoh, M., Usui, T., Kobayashi, S., Tsuchiya, K., Nishikawa, K., Nishikiori, T., Mayumi, T. & Osada, H. (1998). Cell cycle arrest and antitumor activity of pironetin and its derivatives. *Cancer Lett* **126**, 29-32.
4. Kondoh, M., Usui, T., Nishikiori, T., Mayumi, T. & Osada, H. (1999). Apoptosis induction via microtubule disassembly by an antitumour compound, pironetin. *Biochem J* **340 (Pt 2)**, 411-6.
5. Usui, T., Watanabe, H., Nakayama, H., Tada, Y., Kanoh, N., Kondoh, M., Asao, T., Takio, K., Nishikawa, K., Kitahara, T. & Osada, H. (2004). The anticancer natural product pironetin selectively targets Lys352 of alpha-tubulin. *Chem Biol* **11**, 799-806.
6. Banuelos-Hernandez, A. E., Mendoza-Espinoza, J. A., Pereda-Miranda, R. & Cerda-Garcia-Rojas, C. M. (2014). Studies of (-)-pironetin binding to alpha-tubulin: conformation, docking, and molecular dynamics. *J Org Chem* **79**, 3752-64.
7. Prota, A. E., Bargsten, K., Zurwerra, D., Field, J. J., Diaz, J. F., Altmann, K. H. & Steinmetz, M. O. (2013). Molecular mechanism of action of microtubule-stabilizing anticancer agents. *Science* **339**, 587-90.
8. Prota, A. E., Magiera, M. M., Kuijpers, M., Bargsten, K., Frey, D., Wieser, M., Jaussi, R., Hoogenraad, C. C., Kammerer, R. A., Janke, C. & Steinmetz, M. O. (2013). Structural basis of tubulin tyrosination by tubulin tyrosine ligase. *J Cell Biol* **200**, 259-70.
9. Kupchan, S. M., Giacobbe, T. J., Krull, I. S., Thomas, S. M., Eakin, M. A. & Fessler, D. C. (1970). Tumor inhibitors. LVII. Reaction of endocyclic .alpha.,.beta.-unsaturated .gamma.-lactones with thiols. *J Org Chem* **35**, 3539-3543.
10. Marco, J. A., Garcia-Pla, J., Carda, M., Murga, J., Falomir, E., Trigili, C., Notararigo, S., Diaz, J. F. & Barasoain, I. (2011). Design and synthesis of pironetin analogues with simplified structure and study of their interactions with microtubules. *Eur J Med Chem* **46**, 1630-7.
11. Panos, J., Diaz-Oltra, S., Sanchez-Peris, M., Garcia-Pla, J., Murga, J., Falomir, E., Carda, M., Redondo-Horcajo, M., Diaz, J. F., Barasoain, I. & Marco, J. A. (2013). Synthesis and biological evaluation of truncated alpha-tubulin-binding pironetin analogues lacking alkyl pendants in the side chain or the dihydropyrone ring. *Org Biomol Chem* **11**, 5809-26.
12. Desiraju, G. R. (2002). Hydrogen bridges in crystal engineering: interactions without borders. *Acc Chem Res* **35**, 565-73.
13. Janke, C. & Bulinski, J. C. (2011). Post-translational regulation of the microtubule cytoskeleton: mechanisms and functions. *Nat Rev Mol Cell Biol* **12**, 773-86.
14. Zhang, R., Alushin, G. M., Brown, A. & Nogales, E. (2015). Mechanistic Origin of Microtubule Dynamic Instability and Its Modulation by EB Proteins. *Cell* **162**, 849-59.
15. Ravelli, R. B., Gigant, B., Curmi, P. A., Jourdain, I., Lachkar, S., Sobel, A. & Knossow, M. (2004). Insight into tubulin regulation from a complex with colchicine and a stathmin-like domain. *Nature* **428**, 198-202.
16. Gigant, B., Wang, C., Ravelli, R. B., Roussi, F., Steinmetz, M. O., Curmi, P. A., Sobel, A. & Knossow, M. (2005). Structural basis for the regulation of tubulin by vinblastine. *Nature* **435**, 519-22.
17. Prota, A. E., Bargsten, K., Diaz, J. F., Marsh, M., Cuevas, C., Liniger, M., Neuhaus, C., Andreu, J. M., Altmann, K. H. & Steinmetz, M. O. (2014). A new tubulin-binding site and pharmacophore for microtubule-destabilizing anticancer drugs. *Proc Natl Acad Sci U S A* **111**, 13817-21.

18. Andreu, J. M. (2007). Large scale purification of brain tubulin with the modified Weisenberg procedure. *Methods Mol Med* **137**, 17-28.
19. Curmi, P. A., Maucuer, A., Asselin, S., Lecourtois, M., Chaffotte, A., Schmitter, J. M. & Sobel, A. (1994). Molecular characterization of human stathmin expressed in Escherichia coli: site-directed mutagenesis of two phosphorylatable serines (Ser-25 and Ser-63). *Biochem J* **300 (Pt 2)**, 331-8.
20. Kabsch, W. (2010). Xds. *Acta Crystallogr D Biol Crystallogr* **66**, 125-32.
21. Adams, P. D., Afonine, P. V., Bunkoczi, G., Chen, V. B., Davis, I. W., Echols, N., Headd, J. J., Hung, L. W., Kapral, G. J., Grosse-Kunstleve, R. W., McCoy, A. J., Moriarty, N. W., Oeffner, R., Read, R. J., Richardson, D. C., Richardson, J. S., Terwilliger, T. C. & Zwart, P. H. (2010). PHENIX: a comprehensive Python-based system for macromolecular structure solution. *Acta Crystallogr D Biol Crystallogr* **66**, 213-21.
22. Emsley, P. & Cowtan, K. (2004). Coot: model-building tools for molecular graphics. *Acta Crystallogr D Biol Crystallogr* **60**, 2126-32.
23. Karplus, P. A. & Diederichs, K. (2012). Linking crystallographic model and data quality. *Science* **336**, 1030-3.
24. Davis, I. W., Murray, L. W., Richardson, J. S. & Richardson, D. C. (2004). MOLPROBITY: structure validation and all-atom contact analysis for nucleic acids and their complexes. *Nucleic Acids Res* **32**, W615-9.

FIGURE LEGENDS

Figure 1. X-ray structure of the tubulin-pironetin complex.

(**A**) Chemical structures of pironetin in the free and covalently liganded form by Michael addition (nucleophilic addition of a nucleophile to an α,β-unsaturated carbonyl compound) to Cys316 of α-tubulin, respectively.

(**B**) Overall view of the T_2R-TTL–pironetin complex. Tubulin (gray), RB3 (green), and TTL (violetpurple) are shown in ribbon representation. Pironetin (yellow) is depicted in spheres representation and the nucleotides of the individual tubulin chains are shown in sticks representation.

(**C**) Close-up view of the interaction observed between pironetin (yellow sticks) and α-tubulin (gray ribbon). Interacting residues of α-tubulin, including residues shaping the pockets described in the main text, are shown in sticks representation and are labeled.

(**D**) Two views of the pironetin binding pocket in two orientations, highlighting the perfect shape complementarity between the ligand and the pocket. In the right panel, the black arrow points at the O7 atom, which was biotinylated in a previous study[5].

Figure 2. Covalent binding of pironetin to α-tubulin.

(A) Continuous electron density map highlighting the covalent bond between pironetin and Cys316 of α-tubulin. The SigmaA-weighted 2mFo-DFc (grey mesh) and mFo-DFc (green mesh) omit maps are contoured at + 1.0σ and + 3.0σ, respectively. The maps were calculated at an early stage of refinement using a model with an empty binding site.

(**B**) Same electron density maps as in (A) highlighting the disordered side chain of Lys352 of α-tubulin.

(**C**) High performance liquid chromatography (HPLC) trace of intact αβ-tubulin analyzed by MS. Gray trace denotes untreated tubulin, red trace denotes 24 hour treatment with pironetin. Insert shows deconvoluted mass spectra of α-tubulin with treated and untreated conditions colored similarly. Peaks pertaining to the α-tubulin have been shifted by the mass of covalently attached pironetin.

(**D**) Extracted ion chromatogram of the α-tubulin peptide containing Cys316 (residues 306-321) with the addition of pironetin having a measured mass at 2263.155 Da (expected mass: 2263.132 Da).

(**E**) Deconvoluted MS/MS spectra of α-tubulin peptide 306-321 revealing specific pironetin modification at residue Cys316.

Figure 3. Structural changes in tubulin upon pironetin binding.

(**A**) Electron density map highlighting the well-defined secondary structure elements T7 and H8 in the absence of pironetin (PDB ID 4I4T). The SigmaA-weighted 2mFo-DFc (grey mesh) and mFo-DFc (green and red mesh) omit maps are contoured at + 1.0σ and +/- 3.0σ, respectively.

(**B**) Electron density map of the pironetin-liganded complex highlighting the disordered T7 loop and the N-terminal part of helix H8. The same contour levels and colors are used as in (A).

(**C**) Superposition of both the non-liganded (grey) and pironetin-liganded (black) α-tubulin chains in ribbon representation, highlighting the perturbation of helix H8 and the disordered T7 loop (black dashed line). Pironetin and critical residues are in stick representation and are labelled.

Figure 4. Model of the mechanism of action of pironetin on tubulin and microtubules.

(A) Side and top views of the longitudinal tubulin–tubulin contact highlighting the perturbations caused by pironetin in the context of a microtubule. The core atoms of the intermediate domain of the pironetin-liganded α2-tubulin structure of the T_2R-TTL complex (yellow-orange) are superimposed onto the corresponding atoms of an α-tubulin structure derived from a 3.5 Å resolution cryo-electron microscopy reconstruction of a microtubule[14] (PDB ID 3JAL, dark grey). An rmsd of 0.8 Å over 120 C_α atoms was obtained, demonstrating that the α-tubulin intermediate domain undergoes only little structural rearrangements upon the 'curved-to-straight' conformational changes that tubulin dimers must undergo when they assemble into microtubules[15]. For clarity reasons, only the secondary structure elements of α-tubulin forming longitudinal contacts are shown in ribbon representation. β-Tubulin is in light gray surface representation, the α-tubulin side chains forming longitudinal contacts to β-tubulin are in stick representation and are labeled. A hypothetical trace of both the perturbed T7 loop and the N-terminal section of helix H8 is drawn as a dashed yellow-orange line.

(B) Schematic representation of the molecular mechanism of action of pironetin. (1) In the absence of ligands, curved αβ-tubulin heterodimers assemble into microtubules and undergo a curved-to-straight conformational transition. Formation of longitudinal contacts include the interaction between a pocket shaped by loops S3-H3, S5-H5, and H11-H11′ of β-tubulin, and by the T7 loop (black loop) and helix H8 (black knob) of α-tubulin from a neighboring dimer in the microtubule lattice. (2) Pironetin binds to α-tubulin and perturbs the conformation of the T7 loop and helix H8 of α-tubulin (red loop and knob). As a result, pironetin destabilizes microtubules either by forming assembly incompetent tubulin–compound complexes with unassembled tubulin dimers at high ligand concentrations (2), or by binding to the minus ends of microtubules at substoichiometric

ligand concentrations, thus inhibiting the addition of further tubulin dimers (3). The “+” and “–“ signs indicate the microtubule plus- and minus ends, respectively.

Table 1. X-ray data collection and refinement statistics.

	T_2R-TTL-pironetin
Data collection[a]	
Space group	$P2_12_12_1$
Cell dimensions	
a, b, c (Å)	105.7, 157.2, 181.0
Resolution (Å)	48.3 – 2.10 (2.15 – 2.10)
R_{meas} (%)	11.0 (483.0)
R_{pim} (%)	3.2 (139.4)
$CC_{1/2}$[b]	100.0 (23.6)
I/σI	18.9 (0.6)
Completeness (%)	99.9 (99.6)
Redundancy	13.6 (13.0)
Refinement	
Resolution (Å)	48.3 – 2.10
No. unique reflections	175542
R_{work}/R_{free} (%)	18.4 / 23.1
Average B-factors (Å^2)	
Complex	73.2
Solvent	60.9
Ligand (chain C)	62.9
Wilson B-factor	52.2
Root mean square deviation from ideality	
Bond length (Å)	0.007
Bond angles (°)	0.968
Ramachandran statistics[c]	
Favored regions (%)	97.1
Allowed regions (%)	2.8
Outliers (%)	0.1

[a]Highest shell statistics are in parentheses. [b]$CC_{1/2}$= percentage of correlation between intensities from random half-datasets[23]. [c]As defined by MolProbity[24].

SUPPLEMENTAL INFORMATION

Supplemental figure legends

Supplemental Figure S1. MS of α-tubulin peptide 345-366 containing Lys352.

Top trace shows extracted ion chromatogram of the pironetin treated α-tubulin peptide residues 345-366 containing Lys352 showing unmodified peptide having an expected mass at 2388.157 Da. Bottom trace shows identical digest to above extracted for addition of pironetin (2712.387 Da) demonstrating the absence of modified peptide in this mass range. The small peak at 5.31 minutes is a false positive peak that represents the sodium adduct of an unrelated peptide having a mass of 2689.44 Da.

Figure

Figure 1

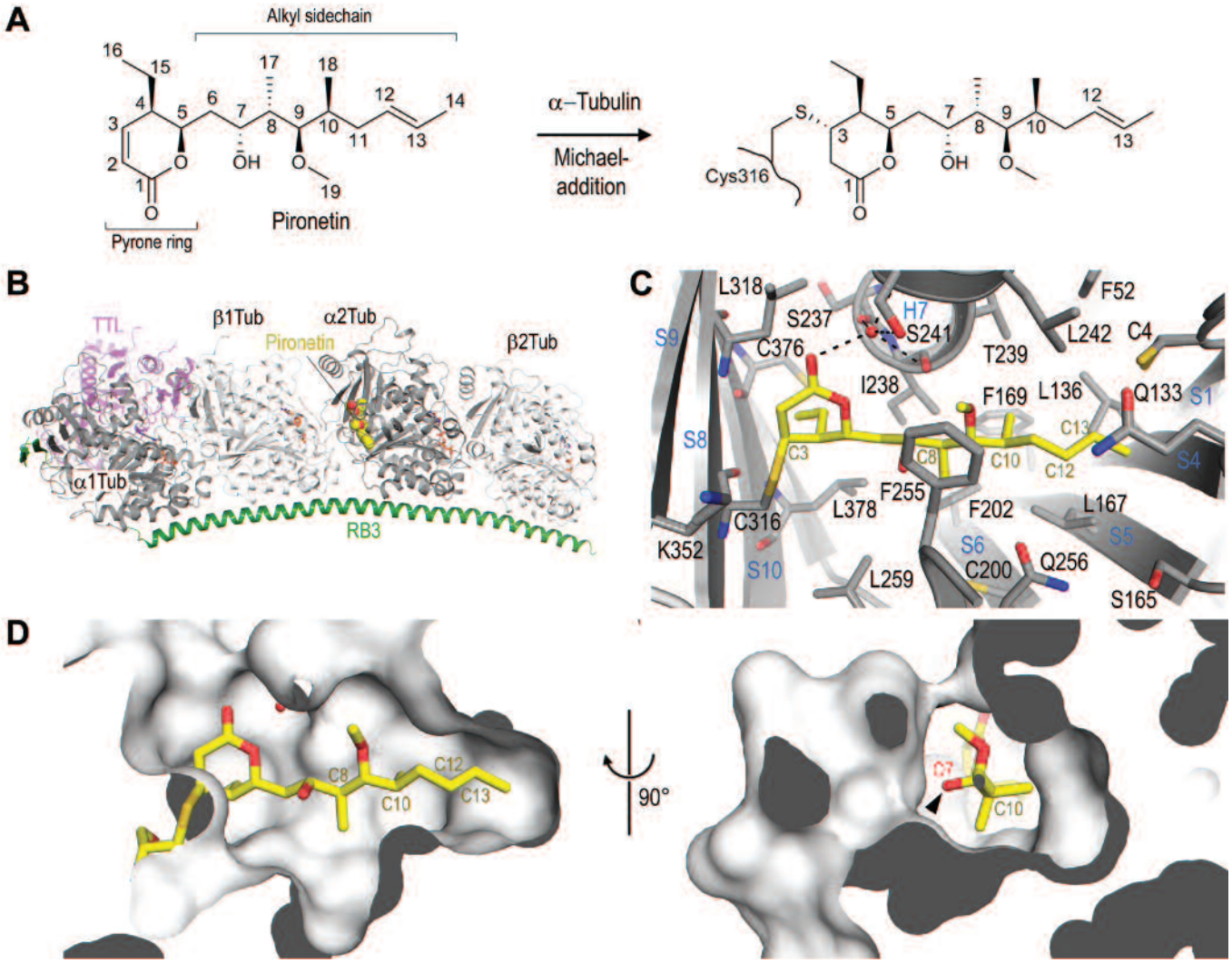

Figure

Figure 2

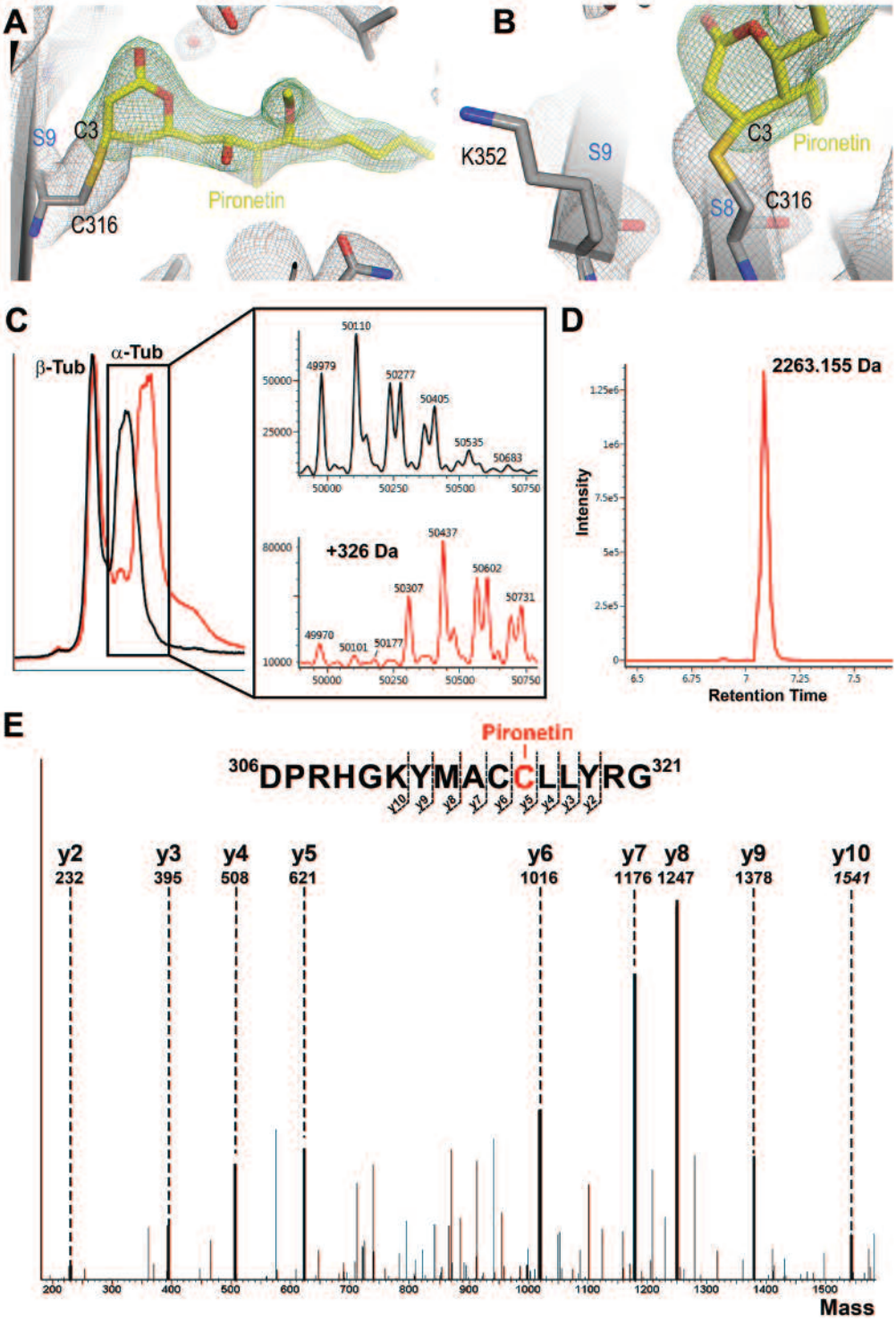

Figure

Figure 3

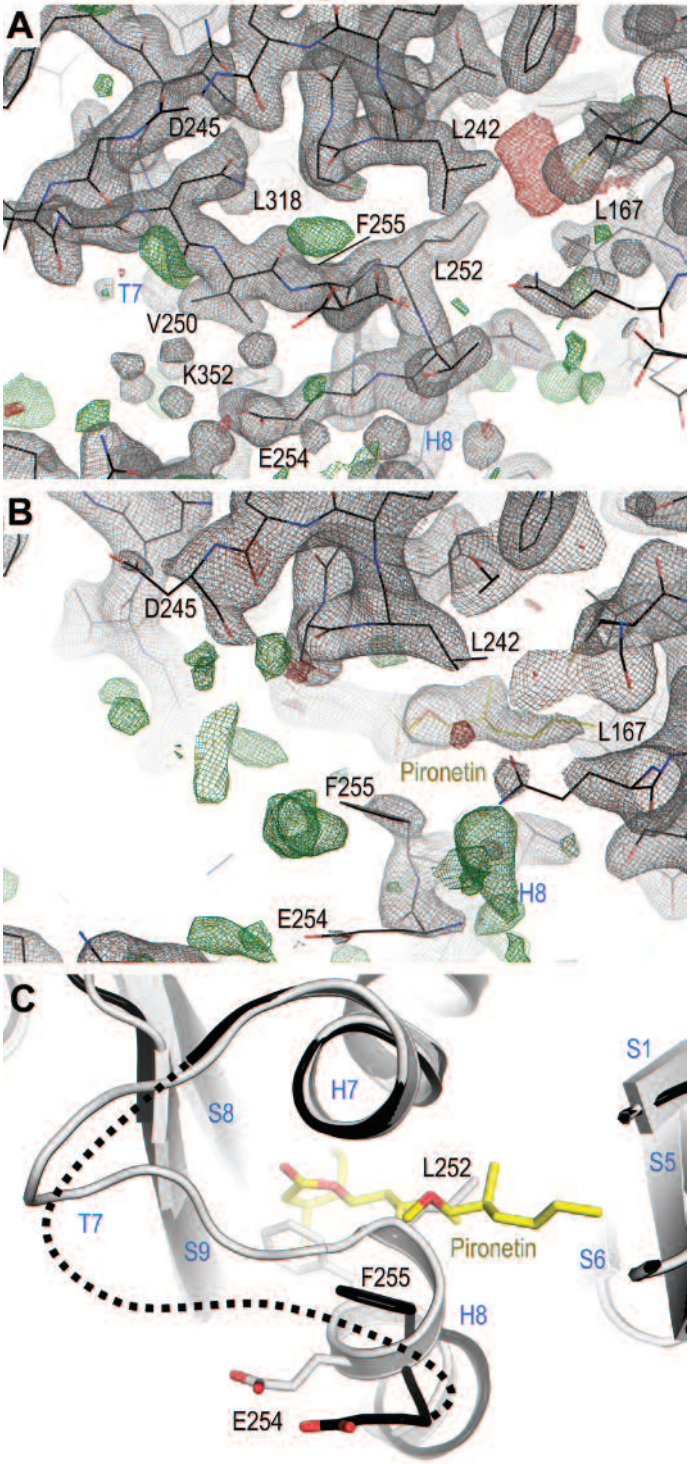

Figure

Figure 4

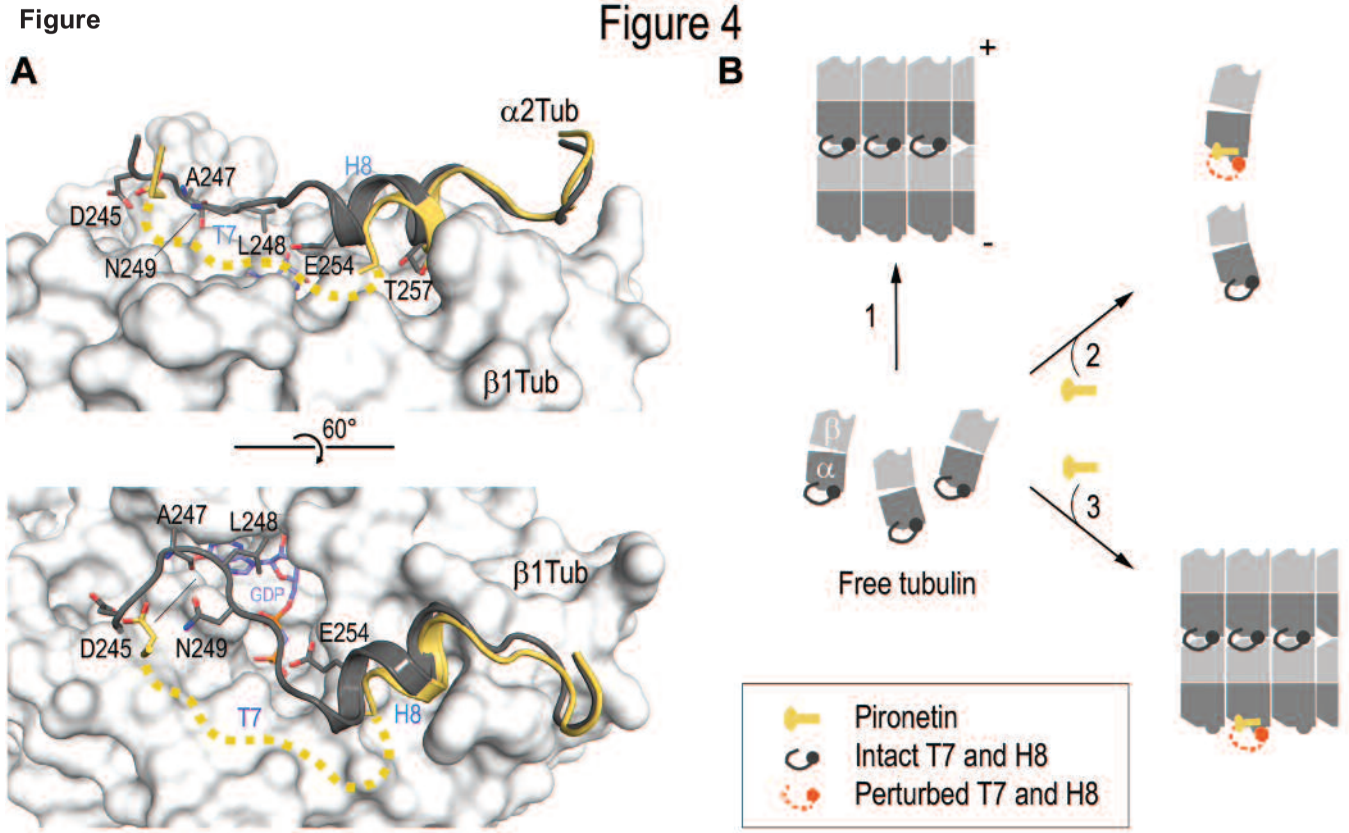

Supplementary Material (To be Published)

Click here to download Supplementary Material (To be Published): Supplemental Figure 1.png